Editors' Suggestion

Observation of Negative Terahertz Photoconductivity in Large Area Type-II Dirac Semimetal $PtTe_2$

Peng Suo,[1,*] Huiyun Zhang,[2,*] Shengnan Yan,[3,*] Wenjie Zhang,[1] Jibo Fu,[1] Xian Lin,[1] Song Hao,[3] Zuanming Jin,[5,6] Yuping Zhang,[2] Chao Zhang,[4] Feng Miao,[3] Shi-Jun Liang,[3,†] and Guohong Ma[1,6,‡]

[1]*Department of Physics, Shanghai University, Shanghai 200444, China*

[2]*College of Electronics and Information Engineering, Shandong University of Science and Technology, Qingdao 266590, China*

[3]*Institute of Brain-inspired Intelligence, National Laboratory of Solid State Microstructures, School of Physics, Collaborative Innovation Center of Advanced Microstructures, Nanjing University, Nanjing, 210093, China*

[4]*School of Physics, University of Wollongong, Wollongong, New South Wales 2522, Australia*

[5]*Terahertz Technology Innovation Research Institute, Terahertz Spectrum and Imaging Technology Cooperative Innovation Center, Shanghai Key Lab of Modern Optical System, University of Shanghai for Science and Technology, 516 JunGong Road, Shanghai 200093, China*

[6]*STU & SIOM Joint Laboratory for Superintense Lasers and the Applications, Shanghai 201210, China*

(Received 7 July 2020; revised 4 February 2021; accepted 21 April 2021; published 4 June 2021)

As a newly emergent type-II Dirac semimetal, platinum telluride ($PtTe_2$) stands out from other two dimensional noble-transition-metal dichalcogenides for the unique band structure and novel physical properties, and has been studied extensively. However, the ultrafast response of low energy quasiparticle excitation in terahertz frequency remains nearly unexplored yet. Herein, we employ optical pump-terahertz probe (OPTP) spectroscopy to systematically study the photocarrier dynamics of $PtTe_2$ thin films with varying pump fluence, temperature, and film thickness. Upon photoexcitation the terahertz photoconductivity (PC) of $PtTe_2$ films shows abrupt increase initially, while the terahertz PC changes into negative value in a subpicosecond timescale, followed by a prolonged recovery process that lasted a few nanoseconds. The magnitude of both positive and negative terahertz PC response shows strongly pump fluence dependence. We assign the unusual negative terahertz PC to the formation of small polaron due to the strong electron-phonon (*e*-ph) coupling, which is further substantiated by temperature and film thickness dependent measurements. Moreover, our investigations give a subpicosecond timescale of simultaneous carrier cooling and polaron formation. The present study provides deep insights into the underlying dynamics evolution mechanisms of photocarrier in type-II Dirac semimetal upon photoexcitation, which is of crucial importance for designing $PtTe_2$-based optoelectronic devices.

DOI: 10.1103/PhysRevLett.126.227402

Introduction.—The emergence of three dimensional (3D) Dirac semimetals (DSMs), a 3D analog of graphene, has lately captured immense attention because of their nontrivial topology properties and the versatile applications in optoelectronic devices [1–6]. With the unique band structures, 3D DSMs show great promise in high-performance photodetection from visible to terahertz spectrum [7–10]. Over the past few years, photoconductive response in DSMs has been studied widely to uncover the photocarrier scattering mechanisms governed by the unique gapless band structure protected by crystalline symmetry [11–14]. With a noninvasive and contact-free feature, terahertz photoconductivity spectrum can be used as a spectroscopic tool to obtain dynamical interaction of various elementary excitations. The negative photoconductivity (NPC) in terahertz frequency spectrum has been widely reported in some materials such as graphene [13,15], Bi_2Se_3 [16,17], as well as MoS_2 [18] and carbon nanotube [19], which were proposed to arise from the role of hot electrons, metallic surface states, and the formation of trions, respectively. Recently, Lorentz-violating type-II Dirac semimetals have been theoretically identified and confirmed experimentally as one type of 3D DSMs, which have tilted anisotropic Dirac cones in momentum space [20–24] and coexisted electron and hole pockets on the Fermi surface [20,25,26]. The distinct band dispersion allows for a unique terahertz PC response in type-II DSMs different from terahertz positive photoconductivity (PPC) in the type-I DSMs [27–29] and terahertz NPC in materials mentioned above.

As a model material of the type-II DSMs, the band structure and transport properties in $PtTe_2$ have been investigated extensively [20,30–35]. However, the study of terahertz PC in the type-II DSM has been seldom reported so far, and the terahertz photoconductive response and associated underlying mechanism remain elusive, although the recent reports demonstrate the tremendous application potential of the DSM $PtTe_2$ in near-infrared imaging and long-wave detection [36,37]. Understanding the dynamical evolution and clarifying the interaction mechanism among different elementary excitations of the type-II DSM $PtTe_2$ after photoexcitation not only provide alternative pathways for controlling electronic energy relaxation and dissipation, which is useful for high-performance optoelectronic devices applications, but also open up an avenue for the further exploration of photo-excited quasiparticles dynamics toward other DSMs and even Weyl semimetals [38,39].

In this Letter, we utilized OPTP spectroscopy to unravel the ultrafast photocarrier dynamics of type-II Dirac semimetal $PtTe_2$ thin film. Our experimental results reveal that the photocarrier responses of $PtTe_2$ thin films initially exhibit absorption enhancement of terahertz radiation induced by hot electron, subsequently, the enhanced terahertz transmission occurs within a subpicosecond timescale, which is rooted in the small polaron formation-induced reduction of carrier mobility. Our study reveals an ideal platform to monitor and engineer the conductivity in terahertz frequency and paves a new way for ultrafast photonic applications.

Sample characterization.—The high-quality films $PtTe_2$ with the thickness of 6.8, 20, and 44 nm and lateral size of 10 mm × 10 mm without intended doping were synthesized on the fused silica substrate, and the detailed process has been provided in our prior work [40]. The detailed thickness and x-ray photoemission spectra of the three films are given in Figs. S1 and S2 of Supplemental Material [41]. Figures 1(a) and 1(b) display the crystal structure of $PtTe_2$ from both the top and side views. The background carrier densities at room temperature are in order of 10^{22} cm^{-3} obtained from Hall measurement for the three films (Fig. S3 in Supplemental Material [41]). Figure 1(c) shows the Raman spectrum of the $PtTe_2$ film with an excitation laser line of 532 nm, two pronounced phonon modes at 112 cm^{-1} (E_g) and 156 cm^{-1} (A_{1g}) are clearly seen for all films, which correspond to the in-plane and out-of-plane vibration mode, respectively. As displayed in Fig. 1(d), the room temperature x-ray diffraction (XRD) pattern measured with grazing incidence exhibits a pronounced (001) characteristic peak for all films, indicating good crystallinity of our samples.

Transient terahertz dynamics measurement.—The time-resolved OPTP experiments in the transmission configuration were performed to explore the dynamics of photocarriers. The optical pulses are delivered from a Ti:sapphire amplifier with 120 femtoseconds (fs) duration at the central wavelength of 780 nm (1.59 eV) and a repetition rate of 1 kHz. The terahertz emitter and detector are based on a pair of (110)-oriented ZnTe crystals. The optical pump and terahertz probe pulse are collinearly polarized with a spot size of 6.5 and 2.0 mm on the surface of the sample, respectively. All measurements were conducted in a dry nitrogen atmosphere, and the samples were placed in a cryostat with the temperature varying from 5 to 300 K.

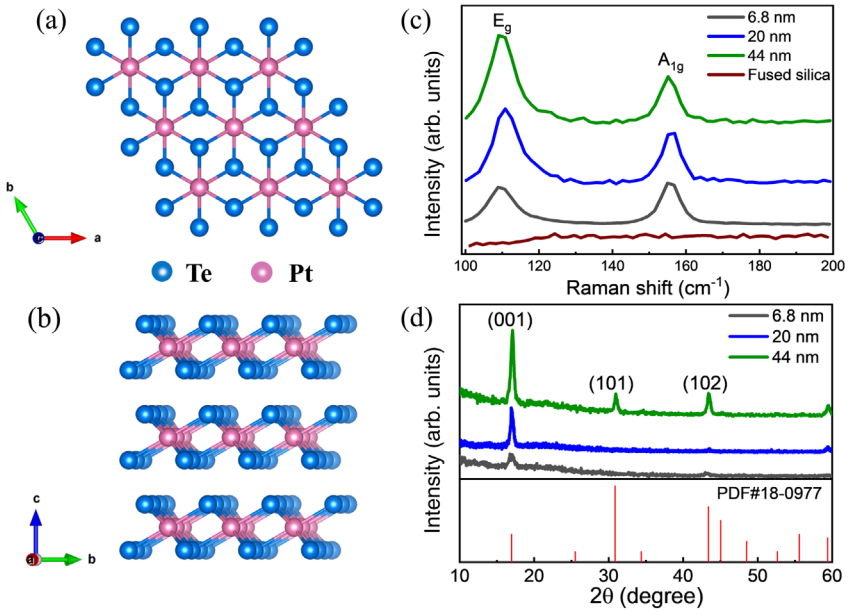

FIG. 1. (a) and (b) show the crystal structure of *ab* and *bc* side view, respectively. (c) Raman spectra and (d) x-ray diffraction pattern of $PtTe_2$ films.

Experimental results.—To probe the photocarrier relaxation of $PtTe_2$ films, we have applied terahertz pulse after an optical pump at 780 nm and measured the photoinduced transmission change, which is defined as $\Delta T = T - T_0$ with respect to the delay time t between terahertz pulse and optical pulse, where the T_0 and T denote the transmission signals of terahertz electric field peak value without and with photoexcitation, respectively. In a thin film approximation, the pump-induced terahertz transmission change $\Delta T/T_0$, is proportional to the terahertz NPC $-\Delta\sigma$ [58]. In the following, the term "film" refers to the 20 nm $PtTe_2$ film on the fused silica substrate unless otherwise stated.

Figure 2 illustrates the pump fluence dependent transient terahertz response of the film at room temperature. Figure 2(a) shows the transient trace $\Delta T/T_0$ as a function of delay time with pump fluence of 542 $\mu J/cm^2$. The inset plots the transient terahertz response in short time window. Fascinatingly, the transient terahertz transmission consists of three stages with distinct timescale: (i) a pump-induced rapid increase in terahertz PC (drop in terahertz amplitude transmission) with response time limited by the laser pulse duration; (ii) the rapid transition in terahertz PC signal from positive to negative on subpicosecond timescale; (iii) the slow recovery process lasts a few nanoseconds from the maximum bleach signal to the equilibrium state. Notably, the transient terahertz response after photoexcitation in the film shows a clear difference from that in type-I DSMs, such as graphene and Cd_3As_2, in which either positive or negative terahertz PC responses were observed [13,15,27,28]. We have also fabricated identical $PtTe_2$ films on sapphire and yttrium aluminum garnet (YAG) substrates. All these films show a similar terahertz response as demonstrated in notes 4 and 5 of Supplemental Material [41].

Figure 2(b) shows the transient terahertz transmission traces under various pump fluences, and the inset presents the magnitude of $\Delta T/T_0$ with respect to the pump fluence at a delay time of $t = 0$ and $t = 3$ ps, respectively. The good linear fluence dependent terahertz transmission indicates that the transient terahertz responses do not exhibit saturation up to 542 $\mu J/cm^2$. Considering that the bleaching signal lasts a few nanoseconds, we employ a monoexponential function convoluted with laser pulse to fit the ultrafast transient terahertz transmission of Fig. 2(b) in the initial 10 ps time window, with the fitting results shown in Fig. S6 of Supplemental Material [41]. The fitting time constants versus pump fluence are presented in Fig. 2(c). The result indicates that the relaxation time of terahertz PC

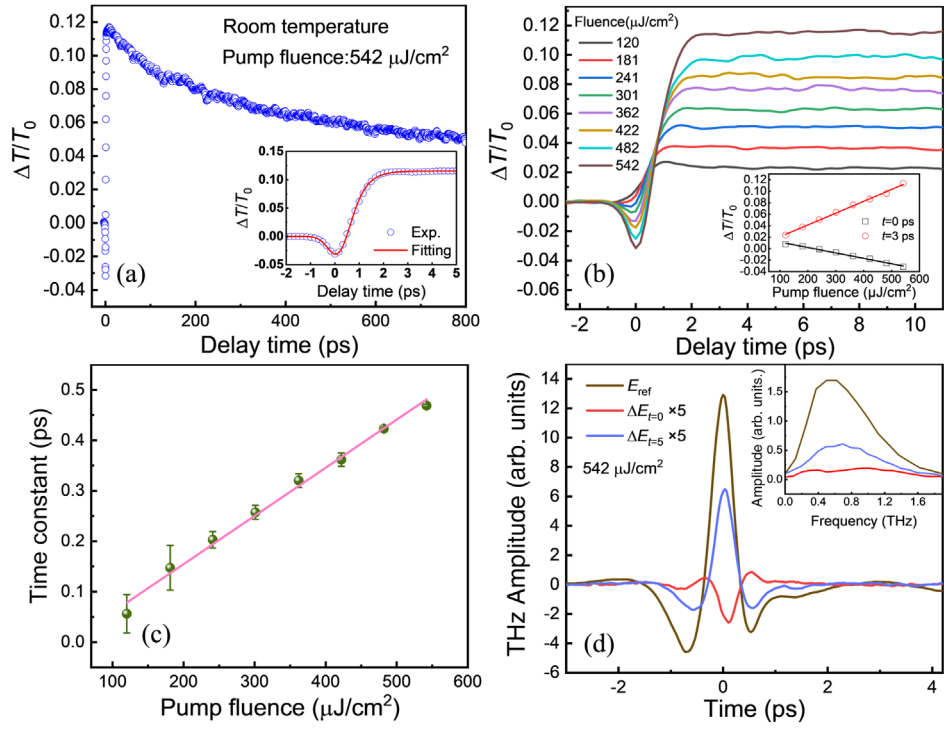

FIG. 2. (a) The transient dynamics of 20 nm $PtTe_2$ film under 780 nm pump at room temperature. The inset plots the transient response in a short time window, the red line is monoexponential fitting. (b) The terahertz transmission, $\Delta T/T_0$, as a function of delay time under various pump fluences. The inset plots the magnitude of $\Delta T/T_0$ at $t = 0$ ps (black) and $t = 3$ ps (red) with respect to pump fluence, respectively. (c) The rising time constants obtained from monoexponential fitting with respect to pump fluence, and the solid line is a linear fitting. (d) Terahertz waveform transmission of the sample without pump (brown) and with pump fluence of 542 $\mu J/cm^2$ collected at delay time $t = 0$ (red) and $t = 5$ ps (blue), respectively. The inset shows the corresponding frequency spectra obtained from Fourier transform.

from positive to negative increases linearly with the applied pump fluence. Figure 2(d) shows the transmitted terahertz waveforms through the film at $t = 0$ ps, 5 ps, and without photoexcitation, respectively. The photoinduced change in the terahertz electric field is expressed as $\Delta E(t_s, t) = E(t_s, t)\text{-}E_{\text{ref}}(t_s)$, where $E(t_s, t)$ and $E_{\text{ref}}(t_s)$ is the time-domain terahertz waveform at t with and without pump, respectively, and t_s is the electro-optical sampling delay for the distinction from the pump-probe delay time t. It is clear that terahertz transmitted waveforms collected at $t = 0$ ps and $t = 5$ ps show out of phase with each other. The relevant frequency-domain spectra via Fourier transform of E_{ref}, $\Delta E_{t=0}$, and $\Delta E_{t=5}$ are shown in the inset of Fig. 2(d).

The film PC, $\Delta\sigma = \Delta(n\mu)e$ with e being elementary charge, is determined by the change of carrier concentration (Δn) and mobility ($\Delta\mu$) under photoexcitation. Thus, the time evolution of terahertz transmission after photoexcitation is governed by Δn and $\Delta\mu$ [15,59]. Compared to the intrinsic high carrier concentration (in the order of 10^{22} cm^{-3}) of the film under studied, the photogenerated carrier density ($\sim 1.8 \times 10^{20}$ cm^{-3} for highest pump fluence) is less than 1% and negligible. The photoexcitation mainly results in the thermalization of electrons through electron-electron (e-e) scattering within a timescale of several tens of fs. The resulting high electron temperature would broaden the Fermi distribution of hot carriers over a wider energy range and lead to free carriers' absorption of terahertz pulses due to the intraband transition undergoes larger possible momentum and energy conservation spaces [28]. Therefore, the photogenerated hot carriers give rise to the sharp enhancement of terahertz absorption in the film. Considering that the bleaching signal appears after a fast relaxation in subpicosecond timescale, the terahertz NPC should only arise from the photoexcitation-induced reduction in carrier mobility. Next, we will discuss origins that may lead to the diminution in carrier mobility of the film.

Discussions.—Before assigning the terahertz NPC to the excitation of small polaron in $PtTe_2$, we discuss other possible origins of the NPC, with more detailed interpretations provided in note 7 in Supplemental Material [41]. In brief, one possible origin of the observed NPC in $PtTe_2$ film could be due to the increased electron effective mass after photoexcitation, which would be true if the electrons in Dirac cones are photoexcited into conduction band under 1.59-eV-optical-excitation. However, it is not the case since the Dirac point in $PtTe_2$ is located around 0.8 eV below the Fermi surface [20,21]. We have carried out OPTP measurement with a pump wavelength of 1600 nm, the pump-induced bleaching of terahertz transmission is still clearly observed as shown in Fig. S7.1 in Supplemental Material [41]. Therefore, the conjecture about the contribution of Dirac electrons can be easily excluded. Another possibility is that the observed NPC in $PtTe_2$ arises from the formation of trions after photoexcitation as in monolayer MoS_2 [18]. Considering the metallic nature of the film with high carrier concentration, the formation of the exciton with photoexcitation can be totally screened by the background free carriers, thus this possibility can be safely ruled out. Third, photoexcitation leading to the elevated lattice temperature may be a possible origin of the observed NPC in $PtTe_2$ film. According to the two-temperature model, the e-e thermalization is much faster than e-ph thermalization after photoexcitation, and the electrons with the elevated temperature transfer the excess energy to lattice via e-ph coupling until the two subsystems reach a balanced temperature [46,49]. The electronic temperature cannot be lower than that before photoexcitation, therefore it is impossible that the observed NPC comes from hot carrier contribution. Besides, $PtTe_2$ films with an identical thickness of 20 nm were grown on various substrates with different thermal conductivities (fused silica, YAG and sapphire), the recovery processes of transient terahertz signals (Fig. S7.2 in Supplemental Material [41]) show almost same relaxation behaviors, which suggests that thermal diffusion cannot explain the long-lived relaxation. Fourth, impurity in the $PtTe_2$ film may also lead to the NPC after photoexcitation as observed in some semiconductors [50–52]. We exclude the contribution of impurity to the NPC based on the following two facts: one is that the terahertz conductivity (without pump) increases with decreasing temperature as shown in Fig. S7.3 of Supplemental Material [41], which indicates the metallic nature of the $PtTe_2$ films and the negligible impurity contribution to terahertz conductivity. The other is that the relaxation time (i.e., a few nanoseconds) of the NPC observed in Fig. 2(a) is 4–6 orders of magnitude faster than the recovering time of the NPC reported in semiconductors [50,51,53,54]. Last but not least, we noted that terahertz radiation on our samples after photoexcitation is negligible so that the observed NPC signal can also rule out the contribution from the photoinduced terahertz radiation. Based on the analyses above, we interpret the unexpected NPC as the photo excitation of small polaron in $PtTe_2$, in which the formation of small polaron leads to the significant reduction of carrier mobility due to the phonon "dressing" of carrier.

The polaron has been experimentally observed in numerous compounds including metal oxides [60,61] and organic semiconductors [62] as well as halide perovskites [63–65]. Besides, the possible existence of polaron formation in graphene and TMDs has been proposed theoretically [66–68]. The strong and short-range e-ph coupling could give rise to the formation of small polaron. Previous experimental measurement [69] has shown that $PtTe_2$ exhibits a strong e-ph interaction with the coupling constant ranging from 0.38 to 0.42. Upon photoexcitation, the photogenerated hot carriers would couple with $PtTe_2$ lattice vibration strongly. It is this strong e-ph coupling that makes the cooling of hot carriers and

distortion of the lattice around the carriers and gives rise to small polaron with reduced carrier mobility, which is the origin of the terahertz NPC. The polaron formation after photoexcitation is supported by the experimental results about the pump fluence dependent NPC shown in Fig. 2(b). Higher pump fluence leads to a higher electron temperature in $PtTe_2$ film, therefore more phonon modes are excited during the hot electron cooling process via e-ph coupling. As a result, more electrons are "trapped" by phonons and the NPC signal under higher pump fluence becomes more pronounced. We also note that the rising time in Fig. 2(c), i.e., the timescale for polaron formation, is within 100–500 fs and is consistent with ~100 fs reported in the conjugated polymers [70] and ~400 fs in the lead-iodide perovskites [63,64].

Since the mobility of small polaron decreases with the reduction of temperature [71,72], we anticipate that a more prominent NPC phenomenon occurs when reducing the temperature of the film. Figure 3(a) plots the $\Delta T/T_0$ collected at $t = 0$ and 3 ps with respect to temperature, respectively, and the inset shows the temperature dependent temporal terahertz transmission at fixed pump fluence of 362 $\mu J/cm^2$. It is clear that the NPC signal at $t = 3$ ps increases monotonously with decreasing temperature, while the PPC signal around $t = 0$ ps is present only at high temperature. When the temperature is lower than 200 K, the PPC behavior vanishes completely. The enhanced NPC signal with decreasing temperature is consistent with the transport property of small polaron. The disappearance of PPC signal around $t = 0$ ps at low temperature suggests that photocarrier thermalization and polaron formation take place simultaneously due to the significant increase of e-ph coupling strength at lower temperature. As a result, the newly formed polaron is "hot," which is composed of hot photocarrier and cold lattice, and subsequent polaron cooling process occurs via e-ph thermalization by transferring the excess energy to deformed lattice. Figure 3(b) shows the transient terahertz dynamics at 5 K for various pump fluences (terahertz dynamics at 100, 200, and 300 K are given in Fig. S8 of Supplemental Material [41]). Apparently, the relaxation of the NPC signal shows an additional fast process with a typical timescale of ~1 ps by comparing with the signal measured at room temperature. The fast relaxation component represents the polaron cooling process, resulting in the increase of polaron photoconductivity. The inset in Fig. 3(b) shows the close-up view of the rising process of the terahertz transmission, and it is clear the rising time increases with pump fluence. Hence, the temperature dependent transient terahertz transmission spectra do support our interpretation that the NPC after photoexcitation in $PtTe_2$ films comes from the formation of small polaron.

We further study the effect of film thickness on the terahertz PC short- and longtime windows at room temperature, with the results shown in Fig. 4. The inset in Fig. 4(a) shows the magnitude ratio of NPC collected at $t = 3$ ps and PPC at $t = 0$ ps, increase of the ratio with the film thickness shows that thicker film exhibits more pronounced negative terahertz PC. Figure 4(b) shows the normalized transient terahertz transmission in a long scan window for the three thickness films, longer relaxation time present in the thicker film indicates slower polaron dissociation process in the thicker film with stronger e-ph coupling. Inset in Fig. 4(b) presents the fitted rising time with respect to film thickness (see Fig. S9 in Supplemental Material [41] for the fitting details). Faster rising time occurring in the thicker film is indicative of larger e-ph coupling in thicker $PtTe_2$ film again, which is reasonable that thicker film has better crystalline as supported by the Raman and XRD results shown in Figs. 1(c) and 1(d), respectively.

We also evaluate the intrinsic conductivity as well as the pump-induced conductivity change of 20 nm $PtTe_2$ film in the investigated terahertz frequency, with results shown in Figs. S10.1 and S10.2 in Supplemental Material [41]. The

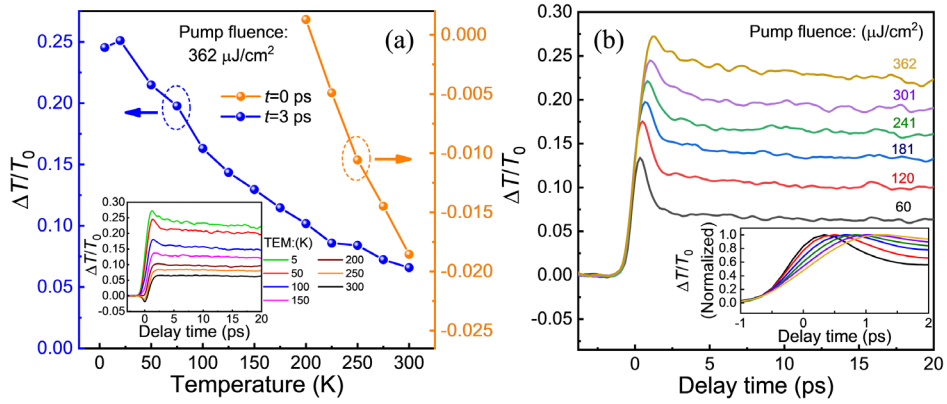

FIG. 3. (a) Temperature dependent $\Delta T/T_0$ at delay time of $t = 0$ ps (orange) and 3 ps (blue), respectively. Inset shows the transient terahertz transmission at various temperatures at fixed pump fluence of 362 $\mu J/cm^2$. (b) The transient terahertz transmission at 5 K under various pump fluences. Inset shows the enlargement of the rising process of $\Delta T/T_0$ under various pump fluences.

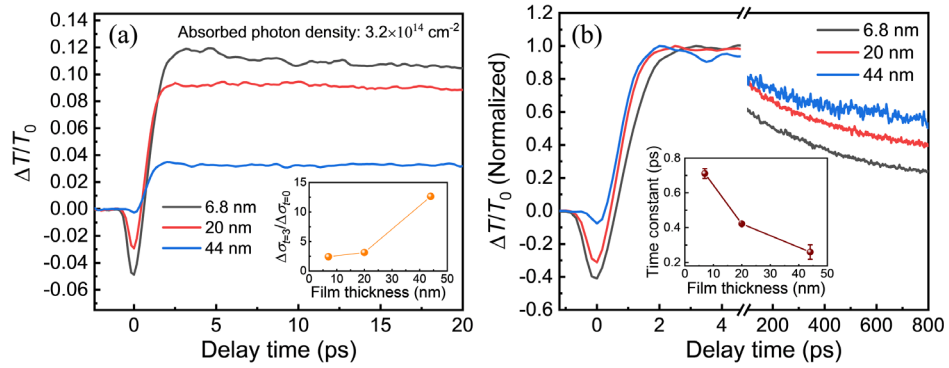

FIG. 4. (a) The transient terahertz transmission for 6.8, 20, and 44 nm $PtTe_2$ films under 780 nm pump at room temperature, the optically injected photon density is 3.2×10^{14} cm^{-2} in all films. Inset plots the magnitude ratio of $\Delta\sigma_{t=3}/\Delta\sigma_{t=0}$ with respect to the film thickness. (b) The normalized terahertz transmission in long scan window for the three films, inset plots the fitting rise time as a function of the film thickness, the solid line is a guide to the eyes.

frequency dependent intrinsic terahertz conductivity in $PtTe_2$ film can be well reproduced with the pure Drude model (see note 10 in Supplemental Material [41] for details), indicating free carrier nature of $PtTe_2$ film in terahertz frequency. Different from the intrinsic terahertz conductivity dispersion, the terahertz photoconductivity at low frequency region is significantly suppressed, manifesting itself in the feature of photocarrier localization effect that takes place after photoexcitation. Similarly, the Drude-Smith model characterizing the carrier localization in the weak confinement system [73] is also employed to analyze the complex terahertz photoconductivity. However, all attempts to fit the $\Delta\sigma$ utilizing the Drude-Smith model fail, which suggests that the photocarriers could be strongly localized. The strong localization of photocarriers further confirms our model of small polaron formation stemming from the photogenerated hot carrier induced lattice deformations in $PtTe_2$ films.

Conclusions.—To summarize, we have utilized ultrafast OPTP spectroscopy to investigate the relaxation dynamics of photoexcited carriers in type-II Dirac semimetal $PtTe_2$ films. The significant feature of the transient terahertz transmission is the enhanced terahertz absorption followed by terahertz photobleach with a lifetime of a few nanoseconds. The fast terahertz response with time constant of hundreds of fs is dominated by simultaneous carriers cooling and formation of small polaron, and the dissociation of small polaron plays a leading role in the recovery process of slow terahertz bleaching. Our investigations offer insights into the photocarriers' dynamics in type-II Dirac semimetal and the new findings may find their implications in the development of novel optoelectronic devices.

This work is supported by the National Natural Science Foundation of China (NSFC, No. 11674213, No. 61735010, No. 11874264, No. 61875106, No. 61775123, No. 61974176, No. 61625402). Science and Technology Commission of Shanghai Municipality (Shanghai Rising-Star Program 18QA1401700), Natural Science Foundation of Jiangsu Province (BK20180330).

*These authors contributed equally to this work.
†To whom correspondence should be addressed.
sjliang@nju.edu.cn
‡To whom correspondence should be addressed.
ghma@staff.shu.edu.cn

[1] S.-Y. Xu, C. Liu, S. K. Kushwaha, R. Sankar, J. W. Krizan, I. Belopolski, M. Neupane, G. Bian, N. Alidoust, T.-R. Chang, H.-T. Jeng, C.-Y. Huang, W.-F. Tsai, H. Lin, P. P. Shibayev, F.-C. Chou, R. J. Cava, and M. Z. Hasan, Science **347**, 294 (2015).
[2] Z. K. Liu, B. Zhou, Y. Zhang, Z. J. Wang, H. M. Weng, D. Prabhakaran, S.-K. Mo, Z. X. Shen, Z. Fang, X. Dai, Z. Hussain, and Y. L. Chen, Science **343**, 864 (2014).
[3] S. Borisenko, Q. Gibson, D. Evtushinsky, V. Zabolotnyy, B. Büchner, and R. J. Cava, Phys. Rev. Lett. **113**, 027603 (2014).
[4] F. Fei, X. Bo, R. Wang, B. Wu, J. Jiang, D. Fu, M. Gao, H. Zheng, Y. Chen, X. Wang, H. Bu, F. Song, X. Wan, B. Wang, and G. Wang, Phys. Rev. B **96**, 041201(R) (2017).
[5] M. Koshino and T. Ando, Phys. Rev. B **81**, 195431 (2010).
[6] Q. Qiu and Z. Huang, Adv. Mater. **33**, 2008126 (2021).
[7] X.-W. Tong, Y.-N. Lin, R. Huang, Z.-X. Zhang, C. Fu, D. Wu, L.-B. Luo, Z.-J. Li, F.-X. Liang, and W. Zhang, ACS Appl. Mater. Interfaces **12**, 53921 (2020).
[8] C. Guo, Y. Hu, G. Chen, D. Wei, L. Zhang, Z. Chen, W. Guo, H. Xu, C.-N. Kuo, C. S. Lue, X. Bo, X. Wan, L. Wang, A. Politano, X. Chen, and W. Lu, Sci. Adv. **6**, eabb6500 (2020).
[9] M. Yang, J. Wang, J. Han, J. Ling, C. Ji, X. Kong, X. Liu, Z. Huang, J. Gou, Z. Liu, F. Xiu, and Y. Jiang, ACS Photonics **5**, 3438 (2018).
[10] Q. Wang, C.-Z. Li, S. Ge, J.-G. Li, W. Lu, J. Lai, X. Liu, J. Ma, D.-P. Yu, Z.-M. Liao, and D. Sun, Nano Lett. **17**, 834 (2017).

[11] C. Zhu, F. Wang, Y. Meng, X. Yuan, F. Xiu, H. Luo, Y. Wang, J. Li, X. Lv, L. He, Y. Xu, J. Liu, C. Zhang, Y. Shi, R. Zhang, and S. Zhu, Nat. Commun. **8**, 14111 (2017).

[12] T. Liang, Q. Gibson, M. N. Ali, M. Liu, R. J. Cava, and N. P. Ong, Nat. Mater. **14**, 280 (2015).

[13] K. J. Tielrooij, J. C. W. Song, S. A. Jensen, A. Centeno, A. Pesquera, A. Zurutuza Elorza, M. Bonn, L. S. Levitov, and F. H. L. Koppens, Nat. Phys. **9**, 248 (2013).

[14] W. Lu, S. Ge, X. Liu, H. Lu, C. Li, J. Lai, C. Zhao, Z. Liao, S. Jia, and D. Sun, Phys. Rev. B **95**, 024303 (2017).

[15] G. Jnawali, Y. Rao, H. Yan, and T. F. Heinz, Nano Lett. **13**, 524 (2013).

[16] R. V. Aguilar, J. Qi, M. Brahlek, N. Bansal, A. Azad, J. Bowlan, S. Oh, A. J. Taylor, R. P. Prasankumar, and D. A. Yarotski, Appl. Phys. Lett. **106**, 011901 (2015).

[17] S. Sim, M. Brahlek, N. Koirala, S. Cha, S. Oh, and H. Choi, Phys. Rev. B **89**, 165137 (2014).

[18] C. H. Lui, A. J. Frenzel, D. V. Pilon, Y.-H. Lee, X. Ling, G. M. Akselrod, J. Kong, and N. Gedik, Phys. Rev. Lett. **113**, 166801 (2014).

[19] M. G. Burdanova, A. P. Tsapenko, D. A. Satco, R. Kashtiban, C. D. W. Mosley, M. Monti, M. Staniforth, J. Sloan, Y. G. Gladush, A. G. Nasibulin, and J. Lloyd-Hughes, ACS Photonics **6**, 1058 (2019).

[20] M. Yan, H. Huang, K. Zhang, E. Wang, W. Yao, K. Deng, G. Wan, H. Zhang, M. Arita, H. Yang, Z. Sun, H. Yao, Y. Wu, S. Fan, W. Duan, and S. Zhou, Nat. Commun. **8**, 257 (2017).

[21] A. Politano, G. Chiarello, B. Ghosh, K. Sadhukhan, C. N. Kuo, C. S. Lue, V. Pellegrini, and A. Agarwal, Phys. Rev. Lett. **121**, 086804 (2018).

[22] T.-R. Chang, S.-Y. Xu, D. S. Sanchez, W.-F. Tsai, S.-M. Huang, G. Chang, C.-H. Hsu, G. Bian, I. Belopolski, Z.-M. Yu, S. A. Yang, T. Neupert, H. T. Jeng, H. Lin, and M. Z. Hasan, Phys. Rev. Lett. **119**, 026404 (2017).

[23] K. Zhang, M. Yan, H. Zhang, H. Huang, M. Arita, Z. Sun, W. Duan, Y. Wu, and S. Zhou, Phys. Rev. B **96**, 125102 (2017).

[24] H.-J. Noh, J. Jeong, E.-J. Cho, K. Kim, B. I. Min, and B.-G. Park, Phys. Rev. Lett. **119**, 016401 (2017).

[25] W. Zheng, R. Schönemann, N. Aryal, Q. Zhou, D. Rhodes, Y. C. Chiu, K. W. Chen, E. Kampert, T. Förster, T. J. Martin, G. T. McCandless, J. Y. Chan, E. Manousakis, and L. Balicas, Phys. Rev. B **97**, 235154 (2018).

[26] J. Zhang and G. Q. Huang, J. Phys. Condens. Matter **32**, 205702 (2020).

[27] W. Zhang, Y. Yang, P. Suo, W. Zhao, J. Guo, Q. Lu, X. Lin, Z. Jin, L. Wang, G. Chen, F. Xiu, W. Liu, C. Zhang, and G. Ma, Appl. Phys. Lett. **114**, 221102 (2019).

[28] W. Lu, J. Ling, F. Xiu, and D. Sun, Phys. Rev. B **98**, 104310 (2018).

[29] Z. Dai, M. Manjappa, Y. Yang, T. C. W. Tan, B. Qiang, S. Han, L. J. Wong, F. Xiu, W. Liu, and R. Singh, Adv. Funct. Mater. **31**, 2011011 (2021).

[30] M.-K. Lin, R. A. B. Villaos, J. A. Hlevyack, P. Chen, R.-Y. Liu, C.-H. Hsu, J. Avila, S.-K. Mo, F.-C. Chuang, and T.-C. Chiang, Phys. Rev. Lett. **124**, 036402 (2020).

[31] K. Deng, M. Yan, C.-P. Yu, J. Li, X. Zhou, K. Zhang, Y. Zhao, K. Miyamoto, T. Okuda, W. Duan, Y. Wu, X. Zhong, and S. Zhou, Sci. Bull. **64**, 1044 (2019).

[32] D. Fu, X. Bo, F. Fei, B. Wu, M. Gao, X. Wang, M. Naveed, S. A. Shah, H. Bu, B. Wang, L. Cao, W. Zou, X. Wan, and F. Song, Phys. Rev. B **97**, 245109 (2018).

[33] L. Fu, D. Hu, R. G. Mendes, M. H. Rümmeli, Q. Dai, B. Wu, L. Fu, and Y. Liu, ACS Nano **12**, 9405 (2018).

[34] O. Pavlosiuk and D. Kaczorowski, Sci. Rep. **8**, 11297 (2018).

[35] J. Lai, J. Ma, Y. Liu, K. Zhang, X. Zhuo, J. Chen, S. Zhou, and D. Sun, 2D Mater. **7**, 034003 (2020).

[36] H. Xu, C. Guo, J. Zhang, W. Guo, C.-N. Kuo, C. S. Lue, W. Hu, L. Wang, G. Chen, A. Politano, X. Chen, and W. Lu, Small **15**, 1903362 (2019).

[37] L. Zeng, D. Wu, J. Jie, X. Ren, X. Hu, S. P. Lau, Y. Chai, and Y. H. Tsang, Adv. Mater. **32**, 2004412 (2020).

[38] S.-Y. Xu *et al.* Science **349**, 613 (2015).

[39] B. Q. Lv, H. M. Weng, B. B. Fu, X. P. Wang, H. Miao, J. Ma, P. Richard, X. C. Huang, L. X. Zhao, G. F. Chen, Z. Fang, X. Dai, T. Qian, and H. Ding, Phys. Rev. X **5**, 031013 (2015).

[40] S. Hao *et al.*, Adv. Funct. Mater. **28**, 1803746 (2018).

[41] See Supplemental Material at http://link.aps.org/supplemental/10.1103/PhysRevLett.126.227402 for details of sample preparation and characterizations, transient terahertz dynamical spectra at different substrates and temperatures, detailed monoexponential fitting, and terahertz conductivity dispersion, which includes Refs. [18–21,42–57].

[42] A. V. Kimel, F. Bentivegna, V. N. Gridnev, V. V. Pavlov, R. V. Pisarev, and T. Rasing, Phys. Rev. B **63**, 235201 (2001).

[43] W. Zhang, J. Guo, P. Suo, L. Lv, J. Liu, X. Lin, Z. Jin, W. Liu, and G. Ma, Appl. Opt. **58**, 8200 (2019).

[44] J. C. Smith, S. Banerjee, V. Pardo, and W. E. Pickett, Phys. Rev. Lett. **106**, 056401 (2011).

[45] N. P. Armitage, E. J. Mele, and A. Vishwanath, Rev. Mod. Phys. **90**, 015001 (2018).

[46] R. H. M. Groeneveld, R. Sprik, and A. Lagendijk, Phys. Rev. B **51**, 11433 (1995).

[47] M. Hase, K. Ishioka, J. Demsar, K. Ushida, and M. Kitajima, Phys. Rev. B **71**, 184301 (2005).

[48] Y. M. Dai, J. Bowlan, H. Li, H. Miao, S. F. Wu, W. D. Kong, P. Richard, Y. G. Shi, S. A. Trugman, J.-X. Zhu, H. Ding, A. J. Taylor, D. A. Yarotski, and R. P. Prasankumar, Phys. Rev. B **92**, 161104(R) (2015).

[49] Y. Ishida, H. Masuda, H. Sakai, S. Ishiwata, and S. Shin, Phys. Rev. B **93**, 100302(R) (2016).

[50] E. Baek, T. Rim, J. Schutt, C. K. Baek, K. Kim, L. Baraban, and G. Cuniberti, Nano Lett. **17**, 6727 (2017).

[51] Y. Yang, X. Peng, H. S. Kim, T. Kim, S. Jeon, H. K. Kang, W. Choi, J. Song, Y. J. Doh, and D. Yu, Nano Lett. **15**, 5875 (2015).

[52] D. Khokhlov, L. Ryabova, A. Nicorici, V. Shklover, S. Ganichev, S. Danilov, and V. Bel'kov, Appl. Phys. Lett. **93**, 264103 (2008).

[53] B. A. Akimov, V. A. Bogoyavlenskiy, L. I. Ryabova, and V. N. Vasilkov, Phys. Rev. B **61**, 16045 (2000).

[54] R. Sreekumar, R. Jayakrishnan, C. Sudha Kartha, and K. P. Vijayakumar, J. Appl. Phys. **100**, 033707 (2006).

[55] A. Thoman, A. Kern, H. Helm, and M. Walther, Phys. Rev. B **77**, 195405 (2008).

[56] S. A. Jensen, *Charge Carrier Dynamics in Photovoltaic Materials* (Universiteit van Amsterdam, Amsterdam, 2014).

[57] N. V. Smith, Phys. Rev. B **64**, 155106 (2001).
[58] F. A. Hegmann, O. Ostroverkhova, and D. G. Cooke, in *Photophysics of Molecular Materials*, edited by G. Lanzani (Wiley-VCH Weinheim, 2006).
[59] J. Lu, H. Liu, and J. Sun, Nanotechnology **28**, 464001 (2017).
[60] M. Ziwritsch, S. Müller, H. Hempel, T. Unold, F. F. Abdi, R. v. d. Krol, D. Friedrich, and R. Eichberger, ACS Energy Lett. **1**, 888 (2016).
[61] A. J. E. Rettie, W. D. Chemelewski, D. Emin, and C. B. Mullins, J. Phys. Chem. Lett. **7**, 471 (2016).
[62] D. Venkateshvaran, M. Nikolka, A. Sadhanala, V. Lemaur, M. Zelazny, M. Kepa, M. Hurhangee, A. J. Kronemeijer, V. Pecunia, I. Nasrallah, I. Romanov, K. Broch, I. McCulloch, D. Emin, Y. Olivier, J. Cornil, D. Beljonne, and H. Sirringhaus, Nature (London) **515**, 384 (2014).
[63] E. Cinquanta, D. Meggiolaro, S. G. Motti, M. Gandini, M. J. P. Alcocer, Q. A. Akkerman, C. Vozzi, L. Manna, F. De Angelis, A. Petrozza, and S. Stagira, Phys. Rev. Lett. **122**, 166601 (2019).
[64] S. A. Bretschneider, I. Ivanov, H. I. Wang, K. Miyata, X. Zhu, and M. Bonn, Adv. Mater. **30**, 1707312 (2018).
[65] K. Miyata, D. Meggiolaro, M. T. Trinh, P. P. Joshi, E. Mosconi, S. C. Jones, F. D. Angelis, and X.-Y. Zhu, Sci. Adv. **3**, e1701217 (2017).
[66] C. Kenfack-Sadem, M. F. C. Fobasso, F. Amo-Mensah, E. Baloitcha, A. Fotué, and L. C. Fai, Physica (Amsterdam) **122E**, 114154 (2020).
[67] B. S. Kandemir, J. Phys. Condens. Matter **25**, 025302 (2013).
[68] Q. Chen, W. Wang, and F. M. Peeters, J. Appl. Phys. **123**, 214303 (2018).
[69] G. Anemone, M. Garnica, M. Zappia, P. C. Aguilar, A. A. Taleb, C.-N. Kuo, C. S. Lue, A. Politano, G. Benedek, A. L. V. d. Parga, R. Miranda, and D. Farías, 2D Mater. **7**, 025007 (2020).
[70] P. B. Miranda, D. Moses, and A. J. Heeger, Phys. Rev. B **64**, 081201(R) (2001).
[71] X.-Y. Zhu and V. Podzorov, J. Phys. Chem. Lett. **6**, 4758 (2015).
[72] C. Franchini, M. Reticcioli, M. Setvin, and U. Diebold, Nat. Rev. Mater. (2021),https://doi.org/10.1038/s41578-021-00289-w.
[73] T. L. Cocker, D. Baillie, M. Buruma, L. V. Titova, R. D. Sydora, F. Marsiglio, and F. A. Hegmann, Phys. Rev. B **96**, 205439 (2017).